Pramāṇa, Vol. 5, No. 1, 1975, pp 1–28. © Printed in India.

Theoretical intensities of low frequency recombination lines

P A SHAVER*
Raman Research Institute, Bangalore 560006

MS received 29 March 1975

Abstract. The possibility of observable recombination lines below 200 MHz is shown to be greatest for the case of negative absorption in low-density gas in front of strong radio sources. The amplification of background radiation can conceivably exceed 100 per cent, especially when the electron temperature is low; on the other hand if the temperature is sufficiently high, dielectronic recombination may give rise to detectable recombination lines from elements other than hydrogen. The optimum frequencies are in the range 50–200 MHz for the interstellar medium, and 1–100 MHz for such intergalactic matter as may exist. The effects of external radiation fields, thermal and nonthermal, are explored quantitatively and the relevant b_n-factors computed for a 1000-level atom; it is found that even the general galactic radiation field will significantly alter the atomic level populations. Observations of these masing low-frequency recombination lines would be useful in sorting out the hot and cold components of the interstellar medium, and in investigating their properties.

Keywords. Recombination lines; interstellar hydrogen; negative absorption; non-equilibrium populations.

1. Introduction

The possibility of negative absorption at radio frequencies has been known for some time. Twiss (1958) wrote " Stimulated transitions are relatively enormously more probable at radio than at optical frequencies and it is this which makes it possible for negative absorption to arise at radio wavelengths when the medium will behave like an amplifier to the incident radiation. " The ratio of stimulated to spontaneous transitions is proportional to

$$\left[\exp\left(\frac{h\nu}{kT_R}\right)-1\right]^{-1},$$

where T_R is the temperature of an equivalent black-body radiation field at frequency ν; at optical frequencies this ratio is generally small ($\ll 1$), but at radio frequencies it can be very large. Twiss restricted his attention to continuum radiation.

Goldberg (1966) was the first to consider the possibility of stimulated emission in radio recombination lines, and he emphasized that its importance would be greatest at the lowest frequencies. However until recently theoretical estimates

* Present address: Kapteyn Astronomical Laboratory, P.O. Box 800, Groningen, The Netherlands.

of low-frequency line intensities were not possible because the necessary non-equilibrium atomic level populations were not known.

It is the purpose of this paper to present calculations of these populations which take into account both thermal and nonthermal radiation fields, to use these results in a study of the quantitative behaviour of recombination lines at low frequencies, and to suggest a low-frequency programme of line observations.

The paper is divided into eight parts. In section 2 atomic level populations are computed for low-density plasmas in the presence of external radiation fields. Section 3 deals with the equations which determine the emission and absorption coefficients, and section 4 with the equations of transfer. In section 5 the parameters of seveal representative model plasma clouds are discussed, and in sections 6 and 7 the results of a series of computations of line intensities based on these models are presented for hydrogen and for other elements respectively.

2. Atomic level populations

The line strengths and absorption coefficients of the gas depend critically on the relative populations of the atomic energy levels. The number of atoms in a given level n is

$$N_n = b_n N_n^* \tag{1}$$

where b_n is a factor introduced by Menzel (1937) to allow for departures from (local) thermodynamic equilibrium (LTE), and the equilibrium population is given by the Saha-Boltzmann equation,

$$\begin{aligned} N_n^* &= N_e N_{x+} \left(\frac{h^2}{2\pi m_e kT_e}\right)^{3/2} \frac{\omega_n}{2} e^{\chi_n} \\ &\approx 4{\cdot}14 \times 10^{-16} \frac{N_e N_{x+}}{T_e^{3/2}} \frac{\omega_n}{2} e^{\chi_n} \text{ cm}^{-3} \end{aligned} \tag{2}$$

Here N_e (cm^{-3}) is the electron density and N_{x+} the ionic density for the element X. T_e (K) is the electron temperature, ω_n is the statistical weight for level n ($\omega_n = 2n^2$ for hydrogen), and

$$\begin{aligned} \chi_n &= hRcZ^2/n^2kT_e \\ &\approx 1{\cdot}58 \times 10^5 Z^2/n^2\, T_e \end{aligned} \tag{3}$$

In the equations $R = 109737{\cdot}31/(1 + m_e/M_x)$ cm^{-1} is the Rydberg constant, m_e and M_x are the electronic and nuclear masses respectively, and the other constants have their usual meaning.

The crucial b_n-factors are determined ultimately by collisional interactions of the atom with the rest of the plasma, and by the ambient radiation field. Strong collisional coupling with the plasma tends to thermalise the higher energy levels, and bring the corresponding b_n-values closer to unity. The effect of a strong external radiation field is similar, but will depend on the detailed character of the field. It is especially important to know whether the level populations will saturate (*i.e.* assume equilibrium values) in the presence of a strong radiation field, thus rendering the maser ineffective.

The relative importance of a radiation field in the absence of collisions can be visualised in the following way. The number of spontaneous transitions from upper level m to lower level n (per cm^3 per sec) is

$$S_{m,n} = N_m A_{m,n} \tag{4}$$

where $A_{m,n}$ is the Einstein coefficient of spontaneous emission. The net number of induced transitions downwards (per cm^3 per sec) is

$$\begin{aligned} I_{m,n} &= (N_m B_{m,n} - N_n B_{n,m}) I_\nu \\ &= \left(\frac{N_m}{\omega_m} - \frac{N_n}{\omega_n}\right) \omega_m I_\nu \frac{c^2}{2h\nu^3} A_{m,n} \end{aligned} \tag{5}$$

Here $B_{m,n}$ and $B_{n,m}$ are the Einstein-B coefficients for induced emission and absorption:

$$B_{m,n} = \frac{c^2}{2h\nu^3} A_{m,n} \tag{6}$$

and

$$B_{n,m} = \frac{\omega_m}{\omega_n} B_{m,n} \tag{7}$$

$\nu\,(= \nu_{m,n})$ is the frequency corresponding to the separation between the two levels, and I_ν is the intensity of the radiation at that frequency impinging on the atoms,

$$I_\nu = W_\nu \frac{2h\nu^3}{c^2} \frac{1}{\exp\left(\frac{h\nu}{kT_R}\right) - 1} \tag{8}$$

T_R is the equivalent black-body temperature of the source of the radiation at frequency ν, and W_ν is the dilution factor defined by

$$W_\nu = \frac{\Omega}{4\pi} \tag{9}$$

where Ω is the solid angle of the radiating source as seen from the cloud of gas. Using the Boltzmann relation

$$\frac{N_n}{N_m} = \frac{b_n}{b_m} \frac{\omega_n}{\omega_m} \cdot \exp\left(\frac{h\nu}{kT_e}\right) \tag{10}$$

and the assumption $h\nu/kT \ll 1$ and $\triangle b = (b_m - b_n) \ll b_n$, we have from eqs (4), (5) and (8),

$$\begin{aligned} \frac{I_{m,n}}{S_{m,n}} &= W_\nu \left(1 - \frac{N_n}{N_m} \frac{\omega_m}{\omega_n}\right) \left(\exp \frac{h\nu}{KT_R} - 1\right)^{-1} \\ &\approx W_\nu \frac{T_R}{T_e} \left(\frac{kT_e}{h\nu} \frac{\triangle b}{b_m} - 1\right) \end{aligned} \tag{11}$$

It is clear from eq. (11) that a radiation field can usually be ignored when the density and temperature of the plasma are high. However, radiative processes can completely dominate in all other cases, especially when the density and temperature are low. They will be particularly important for the higher energy levels, because it is at the corresponding low frequencies that most astrophysical radio

sources are most intense. In most cases the radio source will appear as a mere pinpoint of radiation to the cloud, the dilution will be large, and the radiation field can again be neglected. However this is clearly not true for the omnipresent nonthermal galactic radiation field. It is therefore important in the study of low-frequency recombination lines that the effects of such radiation fields be known quantitatively.

Dupree (1972 *a*) and Brocklehurst (1973) have treated the case of a strong ambient thermal radiation field in a cold plasma of low density. It is the purpose of this section to investigate the effects of nonthermal radiation fields on such plasmas.

The equation of state for a level n can be written as follows:

$$N_n \left[\sum_{m<n} A_{n,m} + \sum_m (B_{n,m} I_\nu + C_{n,m}) + C_{n,i} \right] = \sum_{m>n} N_m A_{m,n} + \sum_m N_m (B_{m,n} I_\nu + C_{m,n}) + N_e N_x^+ (\alpha_{i,n} + C_{i,n}) \quad (12)$$

The left-hand side represents the rate of depopulation of level n, and the right hand side the rate of population. This equation assumes a statistical distribution of the populations among the 1-states ($b_{n1} = b_n$), an assumption which has been justified by Brocklehurst (1971) and Dupree (1972 *a*) by demonstrating the great effectiveness of elastic collisions in redistributing the angular momentum for the highly excited states ($n \gtrsim 40$); the states $n < 40$ do not affect the higher ones because spontaneous radiative transitions dominate all others for $n < 100$. Only the following processes have been taken into account in the present analysis:

1. Spontaneous emission to lower levels ($N_n \sum_{m<n} A_{n,m}$),
2. cascade from higher levels ($\sum_{m>n} N_m A_{m,n}$),
3. radiative recombination ($N_e N_x + \alpha_{i,n}$),
4. Induced emission and absorption between adjacent levels ($N_n B_{n,n\pm1}$, $N_{n\pm1} B_{n\pm1,n} I_\nu$),
5. collisional transitions to adjacent levels ($N_n C_{n,n\pm1}$, $N_{n\pm1} C_{n\pm1,n}$),
6. collisional transitions to the continuum ($N_n C_{n,i}$),
7. three-body (collisional) recombination ($N_e N_x + C_{i,n}$).

The solution for the atomic level populations is usually given in terms of the b_n-factors. It is thus convenient to rewrite eq. (12) in the following form (Seaton 1964 *a*, Dupree 1969):

$$\sum_{n'=n-1}^{n+1} R_{n,n'} b_{n'} = S_n \quad (13)$$

where

$$R_{n,n-1} = -\frac{\omega_{n-1}}{\omega_n} e^{\chi_{n-1}-\chi_n} (B_{n-1,n} I_\nu + C_{n-1,n}) \quad (14)$$

$$R_{n,n} = \sum_{m<n} A_{n,m} + B_{n,n\pm1} I_\nu + C_{n,n\pm1} + C_{n,i} \quad (15)$$

$$R_{n,n+1} = -\frac{\omega_{n+1}}{\omega_n} e^{\chi_{n+1}-\chi_n} (A_{n+1,n} + B_{n+1,n} I_\nu + C_{n+1,n}) \quad (16)$$

$$S_n = \sum_{m>n+1}^{\infty} b_m \frac{\omega_m}{\omega_n} e^{\chi_m - \chi_n} A_{m,n} + \left(\frac{2\pi m_e k T_e}{h^2}\right)^{3/2} \frac{2}{\omega_n} (e^{-\chi_n}) a_{i,n} + C_{n,i} \quad (17)$$

The coefficients in eq. (13) form a tridiagonal matrix, which lends itself to a particularly simple solution involving a forward elimination and a backward substitution (Dupree 1969). The only complication is the presence of the b_n's in the cascade term of S_n; an iterative procedure is used in which those b_n-factors are first set equal to unity, and after each iteration the new b_n's are used to recompute the cascade term. This procedure is continued until successive sets of b_n's and the values $1 - b_n/b_{n+1}$ agree within one per cent. b_n was assumed to be unity for all levels above $N = 1000$, and the solution was carried out for levels between 10 and 1000.

In the above equations $A_{m,n}$ is the Einstein coefficient for spontaneous emission between upper and lower levels m and n respectively,

$$A_{m,n} = \gamma \frac{Z^4}{m^5} \frac{2m^2 g_{m,n}}{n(m^2 - n^2)}$$

$$\approx 1{\cdot}57 \times 10^{10} \frac{Z^4 g_{m,n}}{nm^5 \left(1 - \frac{n^2}{m^2}\right)} \text{ sec}^{-1} \quad (18)$$

where $\gamma = 7{\cdot}87 \times 10^9$ sec^{-1} and $g_{m,n}$ is the Gaunt correction factor to Kramer's formula; it is of order unity, and for $m \gg n \gg 1$ is given approximately by (Menzel and Pekeris 1935 as corrected by Burgess 1958),

$$g_{m,n} = 1 - 0{\cdot}1728 \frac{1 + \left(\frac{n^2}{m^2}\right)}{n^{2/3}\left(1 - \frac{n^2}{m^2}\right)^{2/3}} - 0{\cdot}0496 \frac{\left(1 - \frac{4}{3}\frac{n^2}{m^2} + \frac{n^4}{m^4}\right)}{n^{4/3}\left(1 - \frac{n^2}{m^2}\right)^{4/3}} \quad (19)$$

The rate coefficient for spontaneous emission to lower levels can be approximated within a few per cent over the range of interest by the following power law:

$$\sum_{m<n} A_{n,m} \approx 3{\cdot}23 \times 10^{10} n^{-4.77} \quad (20)$$

The cascade term can be evaluated by using the actual b_m-values from the last iteration up to $m = N$ (1000 in this case); above N, b_m and the exponential terms are set equal to unity and an average Gaunt factor is introduced, yielding an integrable function (Seaton 1964 *a*, Dupree 1969):

$$\sum_{m=N+1}^{\infty} b_m \frac{\omega_m}{\omega_n} e^{\chi_m - \chi_n} A_{m,n}$$

$$\approx \frac{\gamma \bar{g}}{n^3 e^{\chi_n}} \left[\frac{1}{(N+1)[(N+1)^2 - N^2]} + 2\int_{N+1}^{\infty} \frac{dm}{m(m^2 - n^2)}\right]$$

$$= \frac{\gamma \bar{g}}{n^3 e^{\chi_n}} \left[\frac{1}{(N+1)^3\left[1 - \frac{n^2}{(N+1)^2}\right]} - \frac{1}{n^2} \ln\left(1 - \frac{n^2}{(N+1)^2}\right)\right] \quad (21)$$

where

$$\bar{g} = \tfrac{1}{2}(g_{n+1,\,n} + g_{\infty,\,n}) \tag{22}$$

$\alpha_{i,\,n}$ is the rate coefficient for radiative recombination, and is given by (Seaton 1959)

$$\alpha_{i,\,n} = (2a_0\sqrt{\pi})^3 \gamma Z \frac{\lambda^{1/2}}{n} \chi_n S_n(\lambda)$$

$$\approx 2{\cdot}06 \times 10^{-11} \left(\frac{Z}{nT_e^{\frac{1}{2}}}\right) \chi_n S_n(\lambda) \text{ cm}^3 \text{ sec}^{-1} \tag{23}$$

where $\lambda = n^2 \chi_n$ and the function $\chi_n S_n(\lambda)$ has been evaluated and tabulated by Seaton (1959).

The term for induced emission is given by

$$B_{m,\,n} I_\nu = \frac{c^2}{2h\nu^3} A_{m,n} I_\nu \tag{24}$$

and that for induced absorption follows from eq. (7). The intensity of a simple nonthermal radiation field can be represented by the Rayleigh-Jeans approximation to eq. (8), with

$$T_R = T'_R \left(\frac{\nu}{\nu'}\right)^\alpha \tag{25}$$

T'_R is the effective brightness temperature of the source at frequency ν', and α is the (temperature) spectral index. Equation (24) then becomes

$$B_{m,\,n} I_\nu \approx W_\nu A_{m,\,n} \frac{kT'_R}{h\nu'} \left(\frac{\nu}{\nu'}\right)^{\alpha-1} \tag{26}$$

In the case of a thermal radiation field, the radiation intensity is given by the usual equation of transfer (section 4).

$$I_\nu = W_\nu (1 - e^{-\tau_\nu}) \frac{2h\nu^3}{c^2} (e^{h\nu/kT_e} - 1)^{-1} \tag{27}$$

and the induced emission term becomes

$$B_{m,\,n} I_\nu = W_\nu A_{m,\,n} (1 - e^{-\tau_\nu}) (e^{h\nu/kT_e} - 1)^{-1}$$

$$\approx W_\nu A_{m,\,n} \frac{kT_e}{h\nu} (1 - e^{-\tau_\nu}) \tag{28}$$

τ_ν is the optical depth of the thermal radio source at frequency ν,

$$\tau_\nu = \int_0^s K_\nu \, dS' \tag{29}$$

where S is the path length through the plasma. The continuum (bremsstrahlung) absorption coefficient is given by (Oster 1961)

$$K_c = \frac{N_e N_i}{\nu^2 T_e^{3/2}} \ln \left[\frac{T_e^{3/2}}{\nu} \frac{(2k)^{3/2}}{\gamma^5 m_e^{\frac{1}{2}} \pi Z e^2}\right] \left[\frac{8Z^2 e^6}{3c\,(2\pi)^{\frac{1}{2}}\,(m_e k)^{3/2}}\right], \tag{30}$$

whence the continuum optical depth,

$$\tau_c = 3{\cdot}14 \times 10^{-2} \frac{\text{EM}}{\nu^2 T_e^{3/2}} [1{\cdot}5 \ln T_e - \ln (20{\cdot}18\, \nu)] \tag{31}$$

where

$$\mathrm{EM} = \int_0^s N_e^2 \, \mathrm{d}S$$

is the emission measure, N_i is the total ionic density, and the units are N_e, N_i (cm^{-3}), EM ($\mathrm{pc\ cm}^{-6}$), T_e (K) and ν (GHz). These equations are accurate even for low temperatures, at the low frequencies considered in this work (Gayet 1970, Oster 1970).

$C_{n,m}$ and $C_{m,n}$ are collisional rate coefficients for $n \to m$ and $m \to n$ transitions due to electron-atom collisions. It has been shown by Flannery (1970) that atom-atom collisions can be ignored, even in the largely neutral cold clouds. New cross-sections for electron-atom collisions in low-temperature plasmas have recently become available (Banks *et al* 1973); they are considered to be accurate within 40 per cent, and have been used in evaluating the collisional rate coefficients here.

The excitation cross-sections $\sigma_{n,m}(E)$ are given in analytical form by Banks *et al* (1973):

$$\sigma_{n,m}(E) = \frac{\pi}{2} a_0^2 \frac{n^{10}}{m^3} E^2 \left[C(x_-) - C(x_+)\right]$$

$$\approx 4{\cdot}40 \times 10^{-17} \frac{n^{10}}{m^3} E^2 \left[C(x_-) - C(x_+)\right] \mathrm{cm}^2 \qquad (32)$$

where E is in Rydbergs and the following relations are satisfied:

$$4 \frac{\mathrm{Ryd.}}{n^2} \leqslant E \leqslant 2 \frac{\mathrm{Ryd.}}{n} \quad \text{and} \quad 20 \leqslant n, m \leqslant 1000$$

In the above equations $C(x\pm)$ is given by

$$C(x) = \frac{x^2}{\left(2 + \frac{3}{2}x\right)} \ln\left(1 + \frac{2}{3}x\right), \qquad (33)$$

where

$$x_\pm = \frac{2}{En^2 \left| \left(2 - \frac{n^2}{m^2}\right) \pm 1 \right|}. \qquad (34)$$

The collisional rate coefficients are obtained by integrating these cross-sections over a Maxwellian energy distribution of electrons:

$$C_{n,m} = \frac{1}{\sqrt{\pi m_e}} \left(\frac{2}{kT_e}\right)^{3/2} N_e \int_{E_0}^{\infty} \sigma_{n,m}(E) \, E \mathrm{e}^{-\frac{E}{kT_e}} \, \mathrm{d}E \qquad (35)$$

E_0 is the threshold energy for the $n \to m$ transition. It was found that the results could be approximated by the following expression:

$$C_{n,m+1} = 10^{-5} T_e^{-3/2} \exp\left(-26/T_e^{1/3}\right) N_e n^{5{\cdot}2} \ \mathrm{sec}^{-1} \qquad (36)$$

The accuracy of this equation over the range $100 \leqslant n \leqslant 1000$ and $20 \leqslant T_e \leqslant 1000$ K is 40 per cent, the same as the uncertainty in the cross-sections themselves. The collisional de-excitation rate then follows from the principle of detailed balance,

$$C_{m,n} = \frac{N_n^*}{N_m^*} C_{n,m} \tag{37}$$

$C_{n,i}$ is the rate coefficient for collisional transitions to the continuum, as evaluated from the cross-section for Thompson scattering (Seaton 1964 *a*, Dupree 1969),

$$C_{n,i} = 3{\cdot}45 \times 10^{-5} \frac{N_e n^2}{T_e^{\frac{1}{2}}} \mathrm{e}^{-\chi_n} \sec^{-1} \tag{38}$$

The collisional (three-body) recombination rate is then (again from the principle of detailed balance),

$$C_{i,n} = \frac{N_n^*}{N_e N_{e^+}} C_{n,i} \tag{39}$$

The most important simplification made in this analysis is the neglect of all collisional and induced radiation terms between levels other than adjacent levels. In the case of induced emission, it is easy to show that if $T_R \propto \nu^\alpha$, $n \gg \Delta n$, and $h\nu/kT_R \ll 1$, then

$$B_{m,n} I_\nu \propto n^{-(3\alpha+2)} (\Delta n)^{\alpha-2} \tag{40 a}$$

Hence, for an opaque thermal source, an optically thin thermal source, and a nonthermal source (with $\alpha = -2{\cdot}6$), the ratio of the $\Delta n = 2$ induced emission term to the $\Delta n = 1$ term is 0·25, 0·06, and 0·04 respectively. That is, the $\Delta n = 1$ term is completely dominant, especially for a radiation field due to a nonthermal source or an optically thin thermal source.

The collisional terms depend on Δn approximately as follows:

$$C_{n,m} \propto (\Delta n)^{-3/2} \tag{40 b}$$

At $T_e = 20$ K, the $\Delta n = 2$ terms are 30–40 per cent of the $\Delta n = 1$ terms, and the effect of including all these higher order terms can be substantial-effectively doubling or trebling the collisional rates. However, Dupree (1972 *b*) has shown that even a change of two orders of magnitude in the collisional rates only alters the b_n-factors and the slope of the b_n-curve by a factor of two at most. This is because upward and downward collisional transitions between nearby levels very nearly cancel each other, and the collisional ionization term dominates. To illustrate this effect, one can rewrite eq. (13) in the following form,

$$\begin{aligned} &\sum_{\Delta n} B_{n+\Delta n,n} I_\nu b_n \, \Delta b'_- \left[\left(1 - \frac{\Delta b'_+}{\Delta b'_-}\right) + 3\alpha \frac{\Delta n}{n} \right] \\ &\quad + \sum_{\Delta n} C_{n,n+\Delta n} \Delta b_- \left[\left(1 - \frac{\Delta b_+}{\Delta b_-}\right) + \Delta\chi_- - 7{\cdot}2 \frac{\Delta n}{n} \right] \\ &\quad + b_n C_{n,i} = C_{n,i} \end{aligned} \tag{41}$$

where

$$\Delta b'_\pm = \frac{\Delta b_\pm}{b_n} - \Delta\chi_\pm, \quad \Delta b_\pm = \mp (b_n - b_{n\pm\Delta n})$$

and

$$\Delta\chi_\pm = \pm (\chi_n - \chi_{n+\Delta n})$$

Spontaneous transitions and radiative recombinations have been neglected, and these assumptions made: $\Delta n \ll n$, $\Delta b \ll b$, and $\Delta\chi \ll 1$. The importance of collisional transitions between levels relative to collisional ionizations is indicated by the ratio of the second and third terms; for $\Delta n = 1$ this typically peaks in the range $n \sim 100$–300 at a value considerably less than one per cent. Furthermore, for the low densities and high atomic levels that are of interest, in the present work, external radiation fields tend to dominate the processes which determine the level populations, and it has been shown above that the $\Delta n = 1$ transitions are usually completely dominant.

It is implicitly assumed in these calculations that the atom has an infinite number of quantized levels. In reality there must be some level n beyond which quantized states do not exist. A quantized state will clearly not exist if the rate of depopulation,

$$\Gamma_n = \sum_{m<n} A_{n,m} + \sum_{m} (B_{n,m} I_\nu + C_{n,m}) + C_{n,i} \tag{42}$$

exceeds the orbital frequency of the electron (Brocklehurst and Seaton 1972). Collisional transitions and induced radiative transitions determine the rate of depopulation at high n; equating the corresponding rates ($\sum_{\Delta n} C_{n,n+\Delta n}$ and $\sum_{\Delta n} B_{n,n+\Delta n} I_\nu$ from eqs 26, 36, and 40) with the orbital frequency of the electron gives the following two expressions for n_q,

$$n_q^{8\cdot2} \approx 10^{20} T_e^{3/2} \, e^{26/T_e^{\frac{1}{3}}} / N_e \tag{43 a}$$

and

$$n_q^{8\cdot8} \approx 2 \times 10^{31} / W_\nu T_R' \quad (\alpha = -2\cdot6, \quad \nu' = 100 \text{ mHz}). \tag{43 b}$$

For $T_e = 20$ K and $N_e = 0\cdot05$ cm^{-3}, eq. (43 *a*) gives $n_q \sim 1700$. If the ambient nonthermal radiation field is very strong ($T_R' = 10^5 - 10^6$ K), n_q may be as low as 800–1000; however, usually $T_R' \sim 10^3$ K, so that $n_q \sim 1600$. The level populations calculated assuming an infinite number of quantized states should therefore be reasonably accurate at least up to $n \sim 500$.

The assumption that b_n is unity for all levels above 1000 can be justified by the fact that the b_n values asymptotically approach unity as n increases. The resulting error in the solution up to $n = 500$ is very small; indeed in many cases, $n = 600$ solutions agree with the $n = 1000$ solutions within a few per cent up to $n = 500$, in both the b_n values and $1 - b_n/b_{n+1}$.

In these calculations four cases were considered:

1. no external radiation field.
2. a strong "thermal" continuum radiation field due to an adjacent HII region with EM $= 10^6$ pc cm^{-6}, $T_e = 10^4$ K, and $W_\nu = 0\cdot5$.
3. A nonthermal radiation field due to the general galactic background. A representative value for T_R' of 2000 K at 100 MHz was chosen, based on the galactic map of Landecker and Wielebinski (1970) and the usual value for α was adopted, *i.e.*, $-2\cdot6$. The dilution factor is unity.
4. a strong nonthermal radiation field due to an adjacent supernova remnant with $T_R = 100,000$ K at 100 MHz (a typical value—see Milne 1970), $\alpha = -2\cdot6$ and $W_\nu = 0\cdot5$.

The results are presented in figures 1, 2, and 3, for $T_e = 20$ K and 100 K and a range of densities. It is clear from figure 1 that the radiation fields — even the galactic non-thermal field — can have very significant effects, especially when the density is low. They tend to restore LTE and bring the b_n values closer to unity.

A continuum radiation field due to an HII region is most important at relatively low values of n; at higher energy levels or lower frequencies the field assumes a true blackbody spectrum and its importance diminishes. The nonthermal radiation fields must ultimately become dominant at the higher energy levels, since $B_{n,n+1}I_\nu \propto n^{5.8}$ as $n \to \infty$ (eq. 40) whereas $C_{n,n+1} \propto n^{5.2}$. The presence of a nonthermal radiation field is very similar in its effect to an increase in the electron density; the strong nonthermal field in figure 1 has an effect nearly equal to that of a hundredfold increase in density from 10^{-3} cm^{-3}.

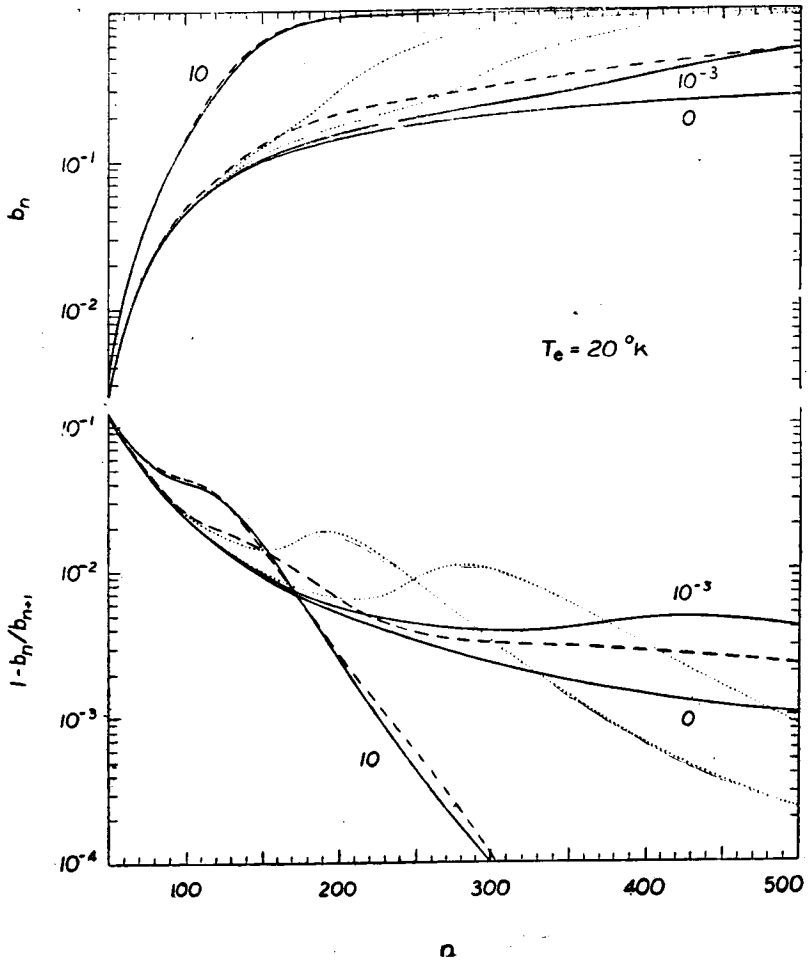

Figure 1. b_n-factors and the slope $\Delta b/b_n$ plotted against principal quantum number n, for $T_e = 20$ K and $N_e = 10$, 10^{-3}, and 0 cm^{-3}. The solid curves represent those cases in which no external radiation field is present, and the dashed and dotted curves represent those cases in which thermal and nonthermal fields respectively are present (for $N_e = 10$ and 10^{-3} cm^{-3} only). The parameters of the fields are given in the text.

In figures 2 and 3 the various curves tend to converge as the density is decreased, because of the increasing relative importance of the galactic non thermal radiation field. The solutions for different densities less than 10^{-3} cm^{-3} are indistinguishable from one another.

It is therefore clear that the level populations will depend on a great many factors external to the plasma cloud. There is evidently no unique set of theoretical b_n-values which will suffice to describe the physical conditions of different low-density clouds in the interstellar medium. However, it is also apparent that even the presence of a very strong radio source contiguous to the cloud will not completely saturate it as far as its masing properties are concerned.

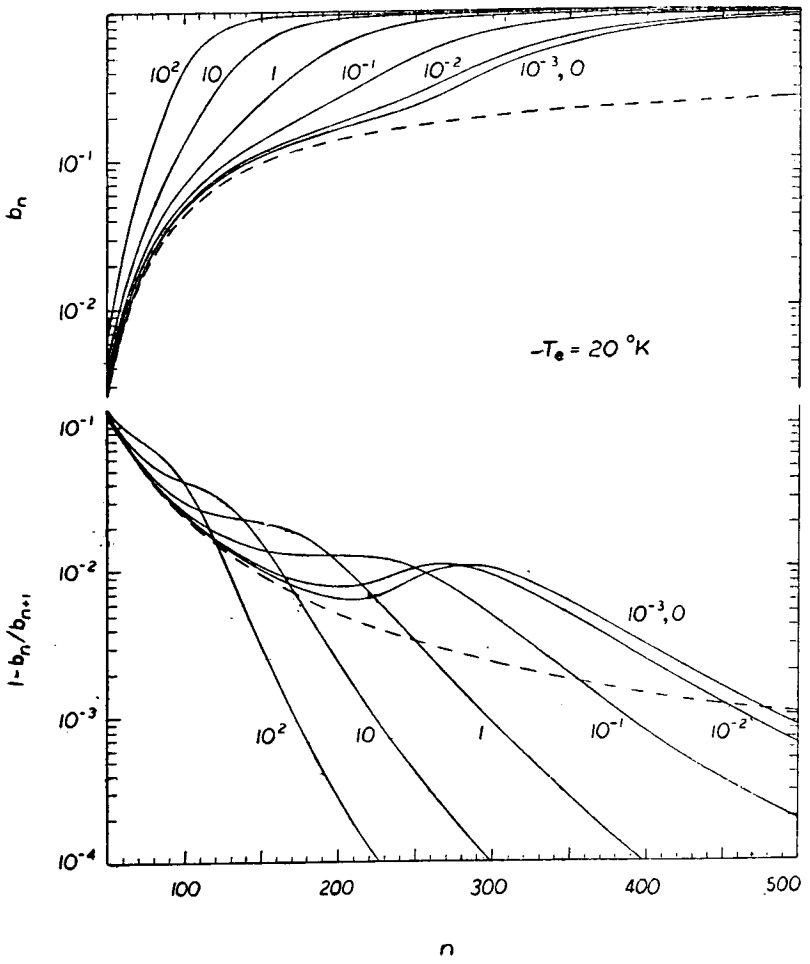

Figure 2. b_n-factors and the slope $\Delta b/b_n$ plotted against principal quantum number n, for $T_e = 20$ K and the densities indicated. The galactic nonthermal radiation field is incorporated in the solid curves (see text for details), and the dashed curve represents the zero-density case with no radiation field present.

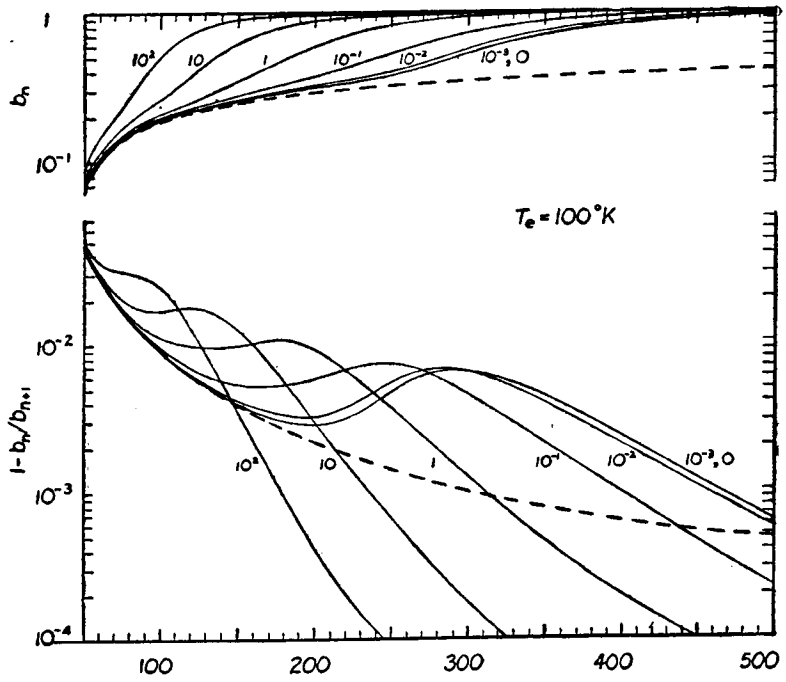

Figure 3. b_n-factors and the slope $\Delta b/b_n$ plotted against principal quantum number n, for $T_e = 100$ K and the densities indicated. The galactic nonthermal radiation field is incorporated in the solid curves (see text for details), and the dashed curve represents the zero-density case with no radiation.

3. Emission and absorption coefficients

The frequency of the transition between upper level m and lower level n is given by the generalised Rydberg formula,

$$\begin{aligned} \nu &= RCZ^2\left(\frac{1}{n^2} - \frac{1}{m^2}\right) \\ &\approx 6{\cdot}58 \times 10^6 \; Z^2 \frac{\Delta n}{n^3}\left(1 - \frac{3}{2}\frac{\Delta n}{n} + \ldots\right) \text{GHz}, \end{aligned} \tag{44}$$

where R is the Rydberg constant defined above, and $\Delta n = m - n$.

The line emission coefficient at frequency ν' can be written

$$\begin{aligned} j_L &= S_{m,n} \frac{h\nu}{4\pi} \phi_{n,m}(\nu') \\ &= N_m A_{m,n} \frac{h\nu}{4\pi} \phi_{n,m}(\nu') \end{aligned} \tag{45}$$

and the absorption coefficient

$$\begin{aligned} K_L &= I_{m,n} \frac{h\nu}{4\pi I_\nu} \phi_{n,m}(\nu') \\ &= \frac{\lambda^2}{8\pi}\left[\frac{N_n}{\omega_n} - \frac{N_m}{\omega_m}\right] \omega_m A_{m,n} \phi_{n,m}(\nu'). \end{aligned} \tag{46}$$

$\phi_{n,m}(\nu')$ is a normalised profile function;

$$\int_{-\infty}^{\infty} \phi_{n,m}(\nu')\,\mathrm{d}\nu' = 1. \tag{47}$$

Equations (45) and (46) can be rewritten explicitly in terms of the b_n-factors, using eqs (1) and (10), as follows,

$$j_L = b_m N_m^* A_{m,n} \frac{h\nu}{4\pi} \phi_{n,m}(\nu') \tag{48}$$

and

$$K_L = \frac{\lambda^2}{8\pi} b_n N_n^* \left[1 - \frac{b_m}{b_n} \mathrm{e}^{-\frac{h\nu}{kT_e}}\right] \frac{\omega_m}{\omega_n} A_{m,n} \phi_{n,m}(\nu') \tag{49}$$

whence the relations between the true emission and absorption coefficients and their equilibrium values,

$$j_L = b_m j_L^* \tag{50}$$

and

$$\begin{aligned} K_L &= b_n \left[\frac{1 - \frac{b_m}{b_n} \mathrm{e}^{-h\nu/kT_e}}{1 - \mathrm{e}^{-h\nu/kT_e}}\right] K_L^* \\ &\approx b_m \left[1 - \frac{kT_e}{h\nu} \frac{\triangle b}{b_m}\right] K_L^* \qquad \left(\frac{h\nu}{kT_e} \ll 1,\ \triangle b = b_m - b_n\right) \\ &\approx b_n \left[1 - \triangle n \frac{kT_e}{h\nu} \frac{\mathrm{d}\ln b_n}{\mathrm{d}n}\right] K_L^* \quad (b_n \gg \triangle b,\ n \gg \triangle n). \end{aligned} \tag{51}$$

It is convenient to express the absorption coefficient in terms of oscillator strength $f_{n,m}$; eq. (46) becomes

$$K_L = \frac{\pi e^2}{m_e c} \left[\frac{N_n}{\omega_n} - \frac{N_m}{\omega_m}\right] \omega_n f_{n,m} \phi_{n,m}(\nu') \tag{52}$$

whence

$$K_L^* = \frac{\pi e^2}{m_e c} \left(\frac{h^2}{2\pi m_e k}\right)^{3/2} \frac{N_e N_{e^+}}{T_e^{3/2}} n^3 (J_{n,m}/n)(1 - \mathrm{e}^{-h\nu/kT_e}) \mathrm{e}^{\chi_n} \phi_{n,m}(\nu') \tag{53}$$

The oscillator strength is given by Kramer's formula modified by the Gaunt correction factor (Menzel 1937):

$$f_{n,m} = \frac{2^6}{3\sqrt{3}\pi} \frac{1}{\omega_n} \frac{1}{\left(\frac{1}{n^2} - \frac{1}{m^2}\right)^3} \left|\frac{1}{n^3} \frac{1}{m^3}\right| g_{m,n} \tag{54}$$

With the assumption $n \gg \triangle n$ this becomes (Menzel 1968)

$$f_{n,m}/n = K(\triangle n)\left[1 + \frac{3}{2} \frac{\triangle n}{n} + \ldots\right] \tag{55}$$

where

$$K(1) = 0{\cdot}1908, \qquad K(2) = 0{\cdot}02633, \qquad K(3) = 0{\cdot}00810 \ldots$$

The line profile is determined principally by Doppler and pressure broadening. In the case of pure thermal Doppler broadening the line shape will be Gaussian,

$$\phi^{\mathrm{D}}_{n,m}(\nu') = \frac{1}{\sqrt{\pi}\,\Delta\nu_{\mathrm{D}}} \exp\left[-\left(\frac{\nu' - \nu}{\Delta\nu_{\mathrm{D}}}\right)^2\right] \tag{56}$$

Here ν is the frequency at the line centre, and $\Delta\nu_{\mathrm{D}}$ is the " Doppler width ", related to the full line width at half-intensity $\Delta\nu_{\mathrm{LD}}$, the kinetic temperature T_e, the "Doppler temperature" T_{D}, the rms turbulent velocity $\langle V_t^2 \rangle^{\frac{1}{2}}$, and the dispersion velocity ΔV by the following expressions,

$$\Delta\nu_D = \frac{\Delta\nu_{\mathrm{LD}}}{2\sqrt{\ln 2}} = \frac{\nu}{c}\left[\frac{2kT_e}{M_{x+}} + \frac{2}{3}\langle V_t^2 \rangle\right]^{\frac{1}{2}} = \frac{\nu}{c}\left[\frac{2kT_{\mathrm{D}}}{M_{x+}}\right]^{\frac{1}{2}} = \frac{\nu}{c}\,\Delta V. \tag{57}$$

In the case of pure pressure broadening the line shape will be approximately Lorentzian (Griem 1967, Peach 1972),

$$\phi^{\mathrm{P}}_{n,m}(\nu') = \frac{\gamma}{\pi}\frac{1}{(\nu' - \nu)^2 + \gamma^2} \tag{58}$$

where $\gamma = \Delta\nu_{\mathrm{LP}}/2$. Griem (1967) showed that, for the low densities prevailing in the astrophysical plasmas under consideration, the pressure broadening is mostly due to collisions (impact effect) rather than to quasi-static electric fields (Stark effect), and that electron impacts are more important than proton impacts. He obtains (for hydrogen)

$$\Delta\nu_{\mathrm{LP}} = \frac{5}{3\sqrt{2\pi}}\left(\frac{\hbar}{m_e}\right)^2\left(\frac{m_e}{kT_e}\right)^{\frac{1}{2}} N_e n^4 \left[\frac{1}{2} + \ln\left(\frac{kT_e\lambda}{3\hbar c n^2}\right)\right] \tag{59}$$

whence

$$\frac{\Delta\nu_{\mathrm{LP}}}{\Delta\nu_{\mathrm{LD}}} = 9{\cdot}74 \times 10^{-16}\,\frac{N_e}{\sqrt{T_e T_{\mathrm{D}}}}\,\frac{n^7}{\Delta n}\left[\ln T_e + \ln\left(\frac{n}{\Delta n}\right) - 11{\cdot}47\right] \tag{60}$$

Brocklehurst and Leeman (1971) have recently computed the profile widths using improved cross-sections, and their result is similar to Griem's:

$$\Delta\nu_{\mathrm{LP}} = 3{\cdot}74 \times 10^{-11}\,\frac{N_e}{T_e^{0{\cdot}1}}\,n^{4{\cdot}4} \quad \mathrm{kHZ}, \tag{61}$$

whence

$$\frac{\Delta\nu_{\mathrm{LP}}}{\Delta\nu_{\mathrm{LD}}} = 7{\cdot}98 \times 10^{-18}\,\frac{N_e}{T_e^{0{\cdot}1}\,T_{\mathrm{d}}^{0{\cdot}5}}\,\frac{n^{7{\cdot}4}}{\Delta n}. \tag{62}$$

When the temperature is low, the assumptions underlying both Griem's work and that of Brocklehurst and Leeman are no longer valid. However, the impact approximation for pressure broadening is still valid for $n \gtrsim 100$ (Griem 1967), so Baranger's (1958) equation (77 *c*) can be used together with the collision rates from section 2 to estimate the line width; Brocklehurst and Leeman have shown that for $n \gg \Delta n$, the line width can then be expressed simply in terms of the damping constant (eq. 42):

$$\Delta\nu_{\mathrm{L}} \approx \frac{1}{2\pi}(\Gamma_m + \Gamma_n) \approx \frac{1}{\pi}\,\Gamma_n \tag{63}$$

(Aller 1953), where m and n are the two levels of the transition. This is an expression of the inverse relation between the lifetimes of the levels and the width of the associated spectral line. The line profile is again Lorentzian (eq. 58) with

$\gamma = (\Gamma_m + \Gamma_n)/4\pi$. When collisions are dominant, the line width is (from eqs 36, 40 *b* and 63)

$$\triangle\nu_{LP} = 2 \times 10^{-8}\, T_e^{-3/2}\, e^{-26/T_e^{\frac{1}{3}}}\, N_e\, n^{5\cdot2} \text{ kHz} \tag{64 a}$$

whence

$$\frac{\triangle\nu_{LP}}{\triangle\nu_{LD}} = 4 \times 10^{-15}\, T_e^{-3/2}\, e^{-26/T_e^{\frac{1}{3}}}\, T_D^{-\frac{1}{2}}\, N_e \frac{n^{8\cdot2}}{\triangle n} \tag{64 b}$$

When a strong radiation field is present, induced transitions may dominate in the damping constant, and therefore also in the line width. In this case the line width is (from eqs 26, 40 *a*, and 63)

$$\triangle\nu_{LP} = 8 \times 10^{-20}\, W_\nu\, T_R'\, n^{5\cdot8} \text{ kHz } (\alpha = -2\cdot6,\ \nu' = 100 \text{ MHz}). \tag{65}$$

When both Doppler and pressure (or radiation) broadening are significant the line profile is given by the convolution of the Gaussian profile with the Lorentzian (a Voigt profile):

$$\begin{aligned}\phi_{n,m}(\nu') &= \int \phi^D_{n,m}(\nu' - \nu'' + \nu)\, \phi^P_{n,m}(\nu'')\, d\nu'' \\ &= \frac{1}{\sqrt{\pi}\ \triangle\nu_D} H(a, u)\end{aligned} \tag{66}$$

where

$$H(a, u) = \frac{a}{\pi} \int_{-\infty}^{+\infty} \frac{e^{-y^2}\, dy}{a^2 + (u - y)^2} \tag{67}$$

Here $a = \gamma/\triangle\nu_D$, $u = (\nu' - \nu)/\triangle\nu_D$, and $H(a, u)$ is the Voigt function, which is tabulated by Harris (1948) and Posener (1959). In computing profile widths and central intensities it is convenient to make analytic approximations to the Voigt function. It was found that the widths central intensities could be approximated in the transition region within 20 per cent by the following two equations:

$$\triangle\nu_L^2 = \triangle\nu_{LD}^2 + \triangle\nu_{LP}^2, \tag{68}$$

and

$$\frac{1}{\phi_{n,m}(\nu)} = \frac{1}{\phi^D_{n,m}(\nu)} + \frac{1}{\phi^P_{n,m}(\nu)}. \tag{69}$$

The LTE absorption coefficient can now be written explicitly in terms of the profile widths; substituting numerical values for the constants and assuming $h\nu/kT_e \ll 1$, eq. (53) becomes

$$K_L^* = 1\cdot63 \times 10^{-3} \frac{N_e N_{x^+}}{T_e^{5/2}}\, n^3\, \nu\, (f_{n,m}/n)\, e^{\chi_n}\, \phi_{n,m}(\nu') \text{ psc}^{-1} \tag{70}$$

and for $n \gg \triangle n = 1$,

$$K_L^* = 1\cdot92 \times 10^3 \frac{N_e N_{x+}}{\triangle\nu_{LD}\, T_e^{5/2}}\, Z^2\, e^{\chi_n} \left[1 + 1\cdot48 \frac{\triangle\nu_{LP}}{\triangle\nu_{LD}}\right]^{-1} \text{ psc}^{-1} \tag{71}$$

at the line centre, where N_e and N_{x^+} are in cm^{-3}, $\triangle\nu_L$ is in kHz, T_e is in K, and ν is in GHz.

4. Radiative transfer and line intensities

The standard equation for the radiative-transfer problem (Chandrasekhar 1960),

$$\frac{\mathrm{d}I}{\mathrm{d}S'} = j + \frac{I_M}{S} - KI \tag{72}$$

has the following general solution,

$$I = I_0 \mathrm{e}^{-\tau} + \int_0^{\tau} \left(S + \frac{I_M}{\tau}\right) \mathrm{e}^{-\tau'} \, \mathrm{d}\tau' + I_F \tag{73}$$

whence, assuming homogeneity,

$$I = I_0 \mathrm{e}^{-\tau} + \left(S + \frac{I_M}{\tau}\right)(1 - \mathrm{e}^{-\tau}) + I_F \tag{74}$$

Here τ' and τ are the elemental and total optical depths through the cloud (eq. 29). I is the intensity of radiation at a given frequency; I_0 and I_F respectively refer to the radiation originating behind and in front of the cloud, and I_M represents the distributed nonthermal emission in the cloud itself. S is the source function related to the emission and absorption coefficients by

$$S = j/K \tag{75}$$

Under LTE conditions Kirchoff's law holds, and S is equal to the Planck function $B(T_e)$. Using this fact and eq. (50), we then have

$$S = \frac{j_L + j_C}{K_L + K_C} = B(T_e)\left[\frac{b_m \tau_L^* + \tau_C}{\tau_L + \tau_C}\right] \tag{76}$$

where the subscripts L and C refer to the line and continuum respectively. Substituting the temperature equivalents for the intensities in eq. (74), we have for the observed brightness temperature,

$$T = T_0 \, \mathrm{e}^{-(\tau_L + \tau_C)} + \left[\frac{T_e (b_m \tau_L^* + \tau_C) + T_M}{\tau_L + \tau_C}\right][1 - \mathrm{e}^{-(\tau_L + \tau_C)}] + T_F \tag{77}$$

The "excess" temperature at the line frequency is obtained by subtracting the temperature of the adjacent continuum from eq. (77), thus:

$$\begin{aligned} \Delta T_L = {} & T_0 \left[\mathrm{e}^{-\tau_C}(\mathrm{e}^{-\tau_L} - 1)\right] + T_e \left[\left(\frac{b_m \tau_L^* + \tau_C}{\tau_L + \tau_C}\right)(1 - \mathrm{e}^{-(\tau_L + \tau_C)}) \right. \\ & \left. - (1 - \mathrm{e}^{-\tau_C})\right] \\ & + T_M \left[\frac{1 - \mathrm{e}^{-(\tau_L + \tau_C)}}{\tau_L + \tau_C} - \frac{1 - \mathrm{e}^{-\tau_C}}{\tau_C}\right]. \end{aligned} \tag{78}$$

In the optically thin case ($1 \gg \tau_C \gg |\tau_L| \gg \tau_L^*$) this reduces to the usual expression,

$$\Delta T_L \approx \tau_L^* \left[b_m T_e - b_n \beta \left(\frac{\tau_C}{2} T_e + \frac{1}{2} T_M + T_0\right)\right] \tag{79}$$

whence for $T_0 = T_M = 0$,

$$\frac{\triangle T_L}{\triangle T_L^*} \approx b_m \left[1 + \triangle n \frac{\tau_C}{2} \frac{kT_e}{h\nu} \frac{\mathrm{d} \ln b_n}{\mathrm{d}n}\right], \tag{80}$$

where

$$\beta \equiv 1 - \triangle n \frac{kT_e}{h\nu} \frac{\mathrm{d} \ln b_n}{\mathrm{d}n} \tag{81}$$

In the optically thick case, assuming τ_L to be negative and $|\tau_L| \gg \tau_C \gg \tau_L^* \gg 1$, eq. (78) becomes

$$\triangle T_L \approx T_0 \mathrm{e}^{-\tau_L} - T_e \left[\frac{\tau_C}{\tau_L} \mathrm{e}^{-\tau_L} + 1\right] \tag{82}$$

Thus, an otherwise opaque cloud will feature prominent emission spikes at the line frequency if $|\tau_L| \gg \tau_C$. It will be transparent at the line frequency if $|\tau_L| \approx \tau_C$. A positive value of τ_L will give rise to an absorption feature, although this is likely to happen only at very high frequencies where the lines are weak or at very low frequencies where τ_C is dominant.

5. Model plasma clouds

In order to summarise fully the behaviour of recombination lines at low frequencies, it is helpful to represent the entire spectrum of interstellar plasma clouds by a few simple models. Broadly speaking there are three main categories—HII regions, and the cloud and intercloud components of the interstellar medium.

The macroscopic properties of a large selection of HII regions have been investigated by Shaver and Goss (1970). They found the maximum excitation parameter ($U = RN_e^{2/3}$, where R is the radius of the HII region) for individual HII regions to be 100–200 pc cm^{-2}; electron densities and temperatures were found to be loosely related to each other (Shaver 1970), ranging from upwards of 10^4 cm^{-3} and 10^4 K at one extreme to as low as 10 cm^{-3} and 2000 K at the other (this correlation results largely from density-sensitive collisional de-excitation of the fine-structure levels of the cooling ions). On this basis three representative spherical, homogeneous models (A, B and C) of HII regions have been adopted, and their physical parameters are summarised in table 1. The rms turbulent velocity was taken in all cases to be supersonic—20 km/s—a typical value (Mezger and Hoglund 1967).

Table 1. Physical parameters of model plasma clouds

Model	T_e (K)	N_e (cm^{-3})	S (pc)	$\langle V_t^2 \rangle^{1/2}$ (km/s)	EM (pc cm^{-6})	U (pc cm^{-2})
A	10000	10^4	0·5	20	5×10^7	116
B	5000	$10^{2.5}$	5	20	5×10^5	116
C	2500	10	50	20	5×10^3	116
D	1000	·05	10000	10	25	..
E	20	·05	1000	10	2·5	..

The physical parameters of the cloud and intercloud components of the interstellar medium were adapted from recent models of the ISM (Field *et al* 1969, Hjellming *et al* 1969). The hot, diffuse intercloud component (D) was assumed to have an electron temperature of 1000 K and an electron density of 0·05 cm^{-3} An rms turbulent velocity of 10 km/s was chosen, and the path length was taken to be 10 kpc, representing a third of the diameter of the galaxy and a typical distance to the farther strong radio sources.

For the cold cloud component (E) the same values for electron density and turbulent velocity were used; the electron temperature was taken to be 20 K. An effective path length of 1 kpc was adopted. This gives an emission measure of 2·5 pc cm^{-6} and an optical depth of 0·5 at 80 MHz which is consistent with interstellar absorption in the direction of many galactic supernova remnants (Dulk and Slee 1972); it implies a filling factor of 0·10 and an average cloud diameter of 40 pc if the actual line of sight is 10 kpc and there are 2·5 clouds per kiloparsec (Radhakrishnan and Goss 1972). The profile width and path length are crucial unknowns in this case, and are discussed in more detail below.

The characteristics of the recombination lines were evaluated for each of the models as follows. The profile widths at half-intensity were computed from eqs (57), (61), (64), and (68), and are shown plotted against frequency in figure 4; these differ from the actual line widths, which can be narrowed by masing. The

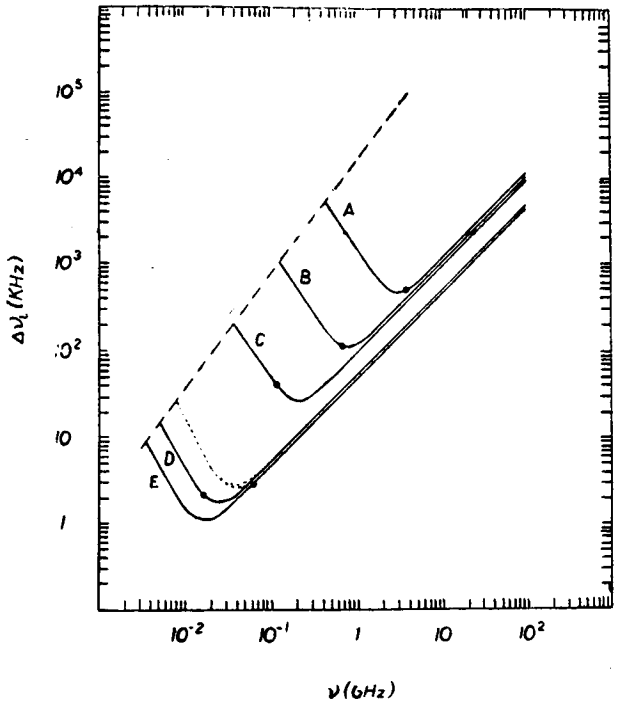

Figure 4. The full profile width at half-maximum intensity, $\Delta\nu_L$, plotted against frequency, for the five cloud models labelled A to E and described in the text. The dashed line shows the distance between the centres of adjacent α-lines and the dot on each curve indicates the frequency at which $\tau_C = 1$ for that model. The dotted curves show the line broadening for models D and E due to radiation damping.

ratio of the line absorption coefficient to its LTE value, K_L/K_L^*, obtained using eq. (51), is shown in figure 5. $\triangle T_L$ and $\triangle T_L^*$ were computed from eq. (78) with $T_0 = T_M = 0$ and are plotted in figure 6. The apparent " amplification factor ", $\exp(-\tau_C)\ [\exp(-\tau_L) - 1]$, from eq. (78), is shown in figure 7.

In all of this work only hydrogen lines ($n + 1 \rightarrow n$ transitions) have been considered; inspection of equations (51) and (53) reveals that higher-order lines will almost invariably be weaker. The temperatures and optical depths all refer only to the line centre and to the line of sight which passes through the centre of the cloud; no allowance has been made for the effects of finite instrumental resolution, which can account for differences of orders of magnitude between the values shown here and actual measurements. The helium content was taken to be ten per cent, so that $N_{H+} = 0{\cdot}09\ N_e$. The b_n-values used for models A, B, and C are from the work of Brocklehurst (1970) with minor extrapolations; for models D and E they were obtained from section 2 above and incorporate the galactic nonthermal radiation field.

6. Hydrogen recombination line intensities

The transition between the Doppler- and pressure-broadening regimes can be seen clearly in figure 4 as a sharp and well-defined minimum in the line width. At

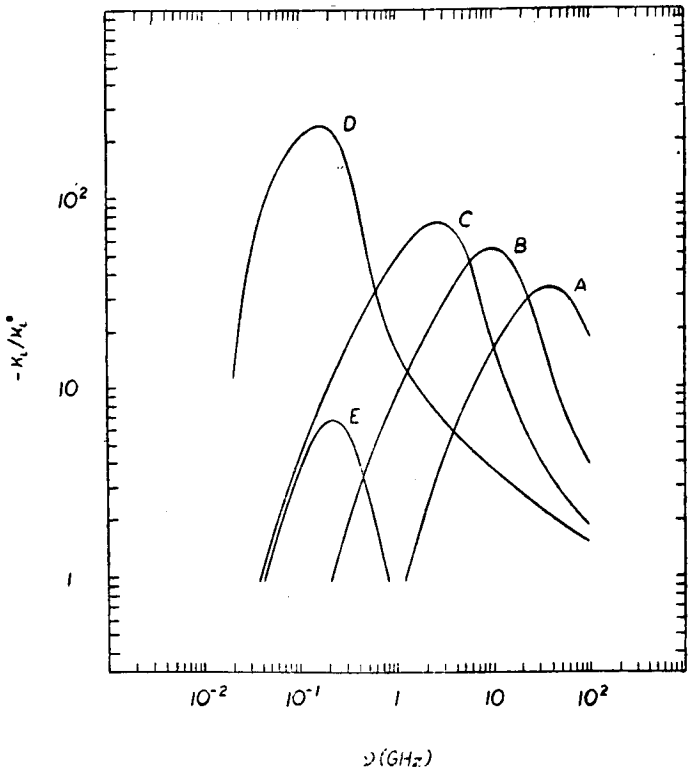

Figure 5. The ratio of the absorption coefficient to its LTE value, K_L/K_L^*, plotted against frequency for the five models labelled A to E and described in the text.

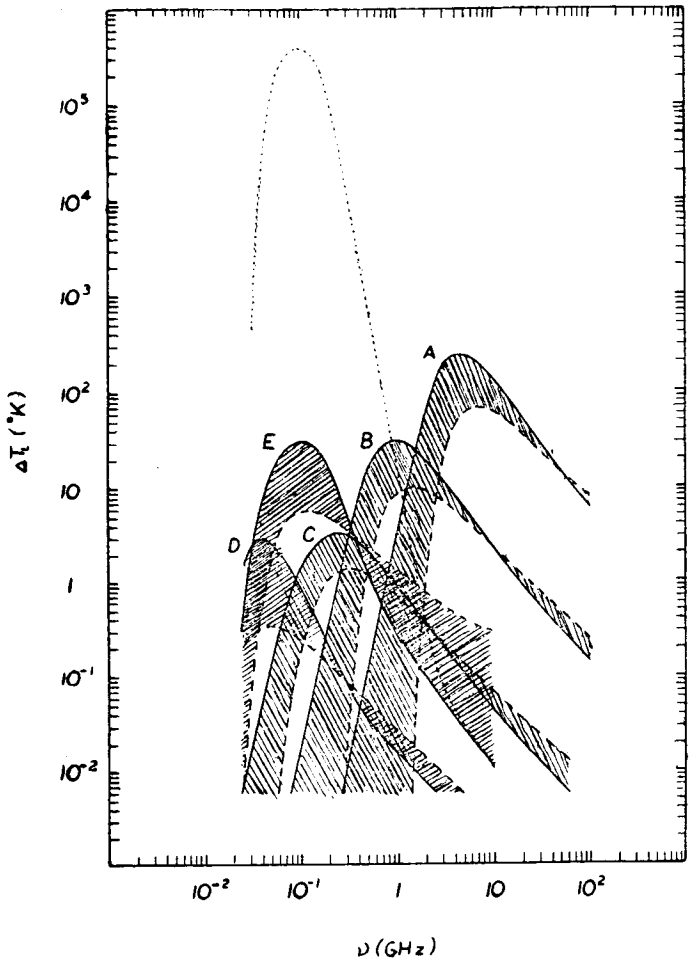

Figure 6. Peak apparent line temperatures plotted against frequency for the five models labelled A to E and described in the text. The solid and dashed curves represent non-LTE and LTE conditions respectively, in the absence of background sources. The dotted curve represents the non-LTE case for model *E*, when there is a strong nonthermal source ($T_R' = 100{,}000$ K at 100 MHz, $\alpha = -2{\cdot}6$) located behind the cloud.

the lower frequencies the profile width is dominated by pressure broadening and increases with decreasing frequency until it becomes equal to the separation between adjacent lines, at which point the lines merge and become indistinguishable. The condition for this to happen can be derived from eqs (44) and (61) for models A, B and C:

$$n_s^{8\cdot4} \approx 5 \times 10^{23}\, T_e^{0\cdot1}\, N_e^{-1} \tag{83}$$

and from eqs (44) and (64) for models D and E:

$$n_s^{9\cdot2} \approx 10^{21}\, T_e^{3/2}\, e^{26/T_e^{1/3}}\, N_e^{-1} \tag{84}$$

The dot on each curve indicates the frequency at which continuum optical depth effects become important; this generally coincides with the frequency at which

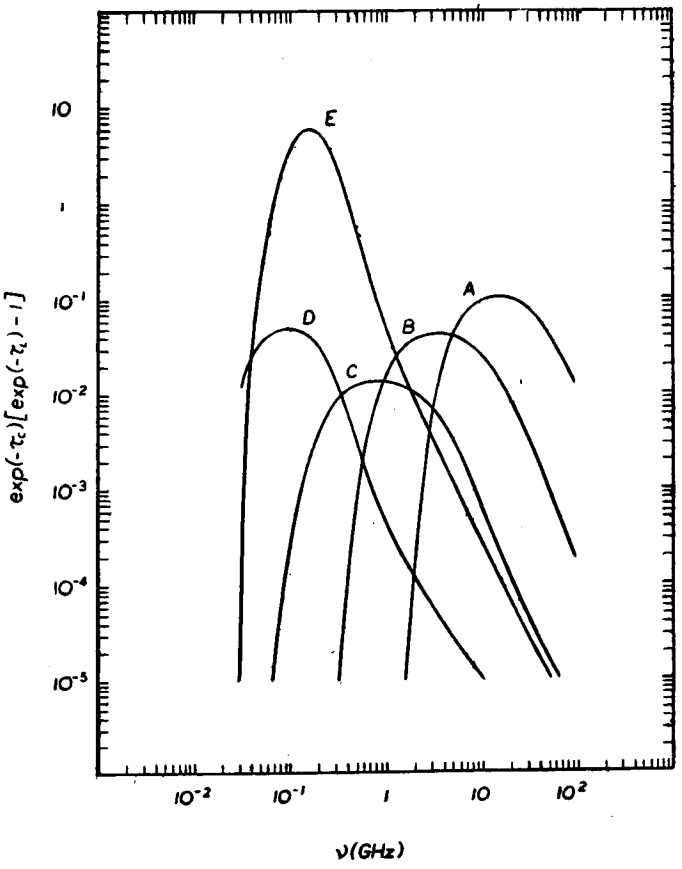

Figure 7. The apparent amplification factor exp $(-\tau_C)$ [exp $(-\tau_L) - 1$] plotted against frequency, for the five models labelled A to E and described in the text.

pressure broadening becomes dominant, making the observation of pressure broadening difficult. The dotted curve shows the effect of the general galactic radiation field for models D and E—in these cases the lines are broadened more by radiation damping than by pressure effects.

The curves in figure 5 show how departures from LTE affect the absorption coefficient and net induced emission ($K_L/K_L^* = I_{m,n}/I_{m,n}^*$). It is striking that the peaks in these curves generally occur at frequencies within an order of magnitude of those at which pressure broadening and optical depth effects become important; all three factors contribute to the weakness of the lines at lower frequencies. It is also clear from figure 5 that the absorption coefficients are most affected by non-LTE effects when the density is low and the temperature high, and at low frequencies.

Figure 6 indicates that the strongest " intrinsic " recombination lines are those due to high-density HII regions, and at frequencies between 1 and 10 GHz. At lower frequencies the dominant lines are due to interstellar gas of lower densities; these lines are not intense, and the problem of detection is further complicated by the high background noise at these low frequencies.

The unusual masing characteristics of these lines do, however, offer a unique solution to the problem of their detection. Figure 7 shows that the amplification of a background signal due to negative absorption at the line frequency can be orders of magnitude greater for the low-density, cold plasmas, and at these low frequencies, than for any of the high-density cases. The low density, the low temperature, and the low frequency at which $\tau_c \gtrsim |\tau_L|$ all conspire to make this so. The line strength, therefore, is only limited by the strength of the background source. Fortuitously it is just at these low frequencies that discrete radio sources, and the general galactic radiation field, are strongest. Narrow lines of great intensity might be observable at the appropriate frequencies; the dotted curve in figure 6 represents one such possible case. Even lines from the hot intercloud component of the interstellar medium should be stronger than any from ordinary HII regions below 200 MHz; one may summarize by saying that the low-density interstellar medium dominates the recombination line spectrum below about 200 MHz, and HII regions above that frequency.

It is convenient at this point to discuss the low-frequency recombination line spectrum of individual classes of plasma separately.

6.1 *HII regions*

It is clear from figure 6 that the intrinsic recombination lines from most HII regions will be very weak below 200 MHz—virtually undetectable in view of the high galactic background. This results from a combination of the three factors—pressure broadening, high continuum opacities, and diminishing deviations from LTE.

However some of the low-density HII regions may still produce detectable recombination lines if they happen to lie along the lines of sight to strong nonthermal sources (figure 7). The minimum detectable temperature for an observation of duration t and bandwidth B may be written

$$\Delta T_{MIN} = 5M \frac{T_0 + T_{SKY} + T_{REC}}{\eta \sqrt{Bt}} \tag{85}$$

where M and η are configuration and efficiency parameters (both of order unity at low frequency). The " system temperature " is comprised of the antenna temperature due to the source (T_0) and sky (T_{SKY}) and the temperature due to the receiver (T_{REC}); at low frequencies the former two are dominant, and if a sufficiently large antenna is used, only T_0 need be considered. The minimum detectable temperature then becomes $\Delta T_{MIN} \sim 5T_0/\sqrt{Bt}$; with a bandwidth of 10 kHz and an integration time of one hour, this is $10^{-3}\ T_0$. Reference to figure 7 indicates that recombination lines from HII regions similar to model C should then be detectable at frequencies somewhat above 100 MHz.

6.2 *The hot intercloud component of the interstellar medium*

Figures 6 and 7 show that recombination lines from the hot, diffuse component of the interstellar medium are only likely to be detectable by virtue of their masing properties. Line stengths of $(1 - 5) \times 10^{-2}\ T_0$ should be possible, depending on the velocity dispersion along the line of sight. The best frequencies lie in the range 50–200 MHz.

6.3 *The cold cloud component of the interstellar medium*

These cold clouds apparently offer the only opportunity for the observation of spectacularly strong recombination lines at low frequencies. Figure 8 shows the amplification factor from eq. (77), $\exp(-\tau_L - \tau_c)$, plotted against frequency for the models A to E; the series of curves for model E represent different electron densities with the emission measure held constant at 2·5 pc cm^{-6}. Enormous amplification is possible, if the density is low enough. The E (0·001, 0) curve is clearly unrealistic in view of the large pathlengths implied. However, it has been included as it represents the limiting case: the magnitude of the observable masing effects cannot be greater, nor the frequency lower, than those indicated by this curve. In particular the condition $\exp(-\tau_L - \tau_c) = 1$ is independent of the emission measure; it can be expressed approximately in the following way,

$$b_n\beta = -3 \times 10^{-5} \frac{T_e^{1.15}\, T_D^{0.5}}{\nu^{1.1}} \qquad (86)$$

where ν is in GHz and T_e and T_D are in K. In the E (0·001, 0) case this equation is also independent of density. The optimum frequency for observing these lines depends on the electron density of the cold clouds; for 0·05 cm^{-3} it is in the vicinity of 100–200 MHz.

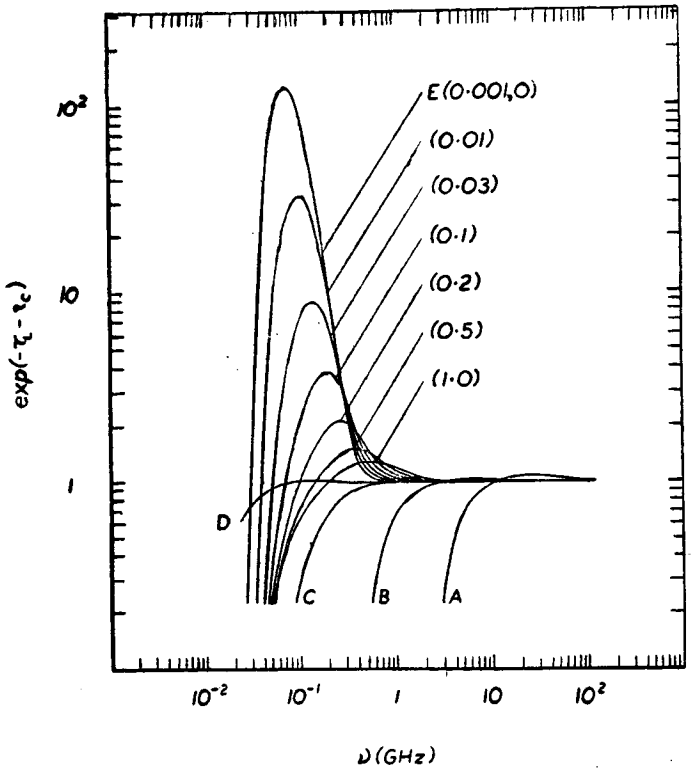

Figur 18. The amplification factor $\exp(-\tau_L - \tau_c)$ plotted against frequency, for the five models labelled A to E and described in the text. The various curves for model E represent different electron densities, as indicated in the brackets; the emission measure has been held fixed at 2·5 cm^{-6}.

The major uncertainties are the effective pathlengths through the cold clouds, and the line broadening and dilution caused by mass motions, systematic and otherwise. These two factors are intimately related to each other. To date several observations above 1 GHz have been made of recombination lines from the general interstellar medium, and the line widths have been typically 30 km/s (Bignell 1973, Cesarsky and Cesarsky 1973, Lockman and Gordon 1973). This value has been used to compute the line properties for a cloud having $N_e = 0{\cdot}05$ cm^{-3} and $T_e = 20$ K and 100 K at 150 MHz; the effective pathlength was left as a free parameter. In figure 9 the effective amplification factor, $\exp(-\tau_L - \tau_c) - \exp(-\tau_c)$ [see eq. (78)], has been plotted against the pathlength; this factor ranges from one per cent to over 100 per cent for pathlengths between 100 and 1000 pc. In view of the great strengths of discrete nonthermal galactic radio sources at this frequency, spectacular line strengths of tens of flux units may be expected if the conditions in the interstellar medium are suitable, and the low-frequency recombination line spectrum of the interstellar medium may be dominated by this cold cloud component.

6.4 *The intergalactic medium*

The above discussion has been concerned with the possibility of low-frequency recombination line emission from hydrogen in the interstellar medium. There remains the further possibility of low-frequency hydrogen recombination lines from the intergalactic medium. The critical cosmological density of matter in the

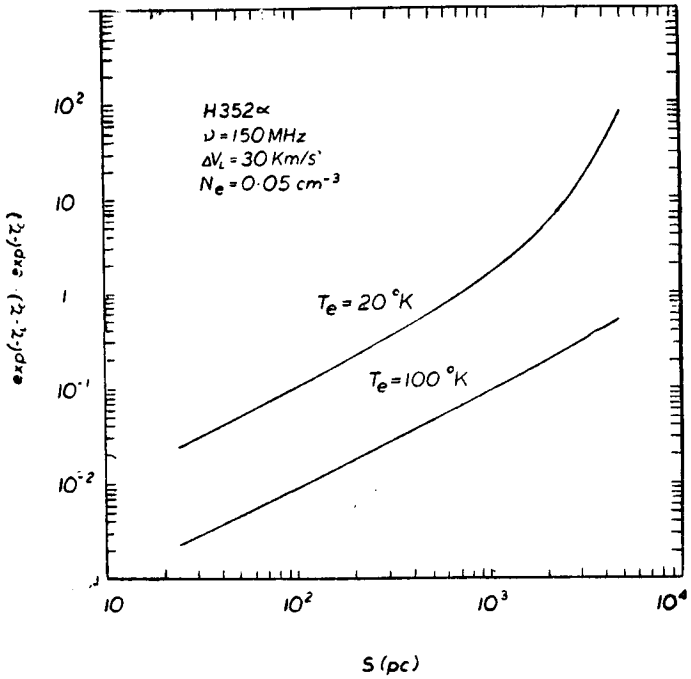

Figure 9. $\exp(-\tau_L - \tau_C) - \exp(-\tau_c)$ plotted against pathlength S, for the H352 α line at 150 MHz and $\Delta V_L = 30$ km/s, $N_e = 0{\cdot}05$ cm^{-3}, He/$H = 10\%$ and $T_e = 20$ and 100 K.

universe ρ_c is proportional to H_0^2, where H_0 is the Hubble constant; for $H_0 = 100$ km sec^{-1} mpc^{-1}, $\rho_c = 2 \times 10^{-29}$ g cm^{-3}, or 1×10^{-5} cm^{-3} in terms of particle density (Field 1972). The width of a spectral line emitted by intergalactic matter is simply $H_0 s$ if the pathlength is great enough; in this case eqs (51) and (71) give

$$\tau_L \approx -9 \times 10^{-9} \frac{H_0^3 \Omega^2}{\nu^2 T_e^{3/2}} b_n \left(\frac{\Delta b}{b_n}\right) \tag{87}$$

for small redshifts, where $\Omega = \rho/\rho_c$. This approximation is valid when $|\beta| \gg 1$, *i.e.*, generally at frequencies below 100 MHz. Presumably the only radiation field involved in this case is the 3 K background, and this would have negligible effect on the atomic level populations; extrapolating the zero-radiation field b_n curves indicates that the line strengths shoud peak in the vicinity of 1–20 MHz. If the electron temperature were as low as 10 K, line intensities of 10 per cent of the background source strength be observable, for $\Omega = 1$. However, it seems highly unlikely that such conditions prevail in the intergalactic medium (Field 1972); the absence of any observable step in the spectrum at the frequency of the 21 cm line of Lyman α makes it virtually certain that the intergalactic medium is highly ionized, and the hypothesis of a cold ionized intergalactic medium is at variance with the lack of observable continuum absorption at very low frequencies. If the intergalactic medium is ionized its temperature is likely to be greater than 10^4 K, and X-ray observations set an upper limit of $\sim 10^8 - 10^9$ K. A temperature of 10^4 K may then be considered the most optimistic value for the detection of low-frequency recombination lines. With approximate b_n-values obtained by extrapolation from the high-temperature cases in section 2 $H_0 = 100$/km sec^{-1} Mpc^{-1}, $\Omega = 1$, $\nu = 10$ MHz, and $T_e = 10^4$ K, $\Delta T_L \approx 5 \times 10^{-8} T_0$. At this frequency the separation between adjacent lines corresponds to only 10 Mpc for $H_0 = 100$ km sec^{-1} Mpc^{-1}, so the lines will overlap for most extragalactic radio sources. Only the step at the line frequency can be detected; a wide bandpass can now be used, and the results averaged for all the lines in the bandpass to increase the signal-to-noise ratio still further. For a total bandwidth of 1 MHz and an integration time of 10 hr a line strength of $10^{-6} T_0$ could in principle be detected. Even this sensitivity is not adequate, and the line strengths diminish rapidly as T_e is increased still further. Thus these lines could only be detected if $\Omega \gg 1$, or if there are substantial density inhomogeneities in the intergalactic medium.

7. Dielectronic recombination onto heavier ions

A hot intergalactic medium, and the hot intercloud component of the interstellar medium, may give rise to detectable recombination lines through the mechanism of dielectronic recombination. The dielectronic recombination coefficient is maximum at temperatures of 10^5–10^6 K; at these temperatures the populations of the higher energy levels can exceed their equilibrium values by a factor of a million, if the density is sufficiently low. The peak of the b_n-curve is located near the level where the rate of spontaneous radiative transitions out of the state equals either the rate of collisional excitation out of the state (Berger and Simon 1972),

$$n_{max}^9 \approx 10^{16} Z^6 T_e^{\frac{1}{2}} N_e^{-1} \tag{88}$$

or the rate of radiatively induced transitions out of the state,

$$n_{\max}^{10\text{-}6} \approx 10^{26}/W_\nu T_R' \tag{89}$$

Below n_{max} the lines will appear in emission, and above it, in absorption.

For a given Doppler temperature, $|\beta| \gg 1$, and $\Delta b \ll b$, where $b_n \propto n^i$. Calculations by Burgess and Summers (1969) indicate that typically $i \sim 1{\cdot}5$ for $n < n_{max}$ and $i \sim -4{\cdot}5$ to $-5{\cdot}0$ for $n > n_{max}$. Hence τ_L increases as $n^{6{\cdot}5}$ below n_{max} (however, the galactic radiation field will cause the b_n's to fall off much faster above n_{max} for the interstellar medium—this factor must be taken into account in any rigorous treatment of the problem). Any lines due to dielectronic recombination will therefore be strongest for $n > n_{max}$, in the absorption regime; as indicated above, it is also at the corresponding low frequencies that T_0 is greatest. The line intensities will finally diminish when b_n approaches unity and the slope of the curve approaches zero.

(*a*) *The interstellar medium.*—The frequency corresponding to n_{max} for α-lines from the interstellar medium (model D) is $\sim$ 1–2 GHz (for $Z = 1$). Below this frequency the optical depth in the line may decrease somewhat with decreasing frequency due to the galactic radiation field; a crude extrapolation of the curves of Burgess and Summers suggests that the b_n-factors will in any case finally approach unity at about 1 MHz. Taking into account other factors such as pressure broadening, continuum absorption, and the frequency dependence of T_0, the optimum frequencies for observing these lines would appear to lie in the range 100–200 MHz.

The temperature of the interstellar medium is too low for dielectronic recombination onto helium to be significant, but other elements are more promising. Burgess and Summers show curves for calcium; taking $T_e = 10^4$ K, $T = 2{\cdot}6 \times 10^4$ K, $s = 10$ kpc, $N_e = 0{\cdot}05$ cm^{-3}, and $N(\mathrm{Ca})/N(H) = 2{\cdot}5 \times 10^{-6}$, the central line optical depth at 100 MHz is estimated to be $\tau_L \sim 2 \times 10^{-4}$. Several other elements are two orders of magnitude more abundant than calcium; considering also that the lines due to carbon and all heavier elements will be merged together in the hydrogenic series due to the widths of the lines, it appears that low-frequency recombination lines from the interstellar medium due to dielectronic recombination may indeed be detectable.

(*b*) *The intergalactic medium.*—For α-lines from an intergalactic medium with $T_e = 10^6$ K and $N_e = 10^{-5}$ cm^{-3}, the frequency corresponding to n_{max} is $\sim$ 100–200 MHz (for $Z = 1$), and the b_n-factors approach unity at frequencies far less than 1 MHz. Allowing once again for pressure broadening, continuum absorption, and the frequency dependence of T_0, the best frequency probably lies in the range 1–100 MHz; confusion with effects due to the interstellar medium presents an additional problem in this case.

The calculations of Burgess and Summers (1969) show that the likely temperature of the intergalactic medium, 10^6–10^7 K, would be optimal for dielectronic recombination onto helium. Unfortunately however almost all of the helium would be in the doubly-ionized state at these temperatures, making the lines extremely weak. From Seaton (1964 *b*),

$$\frac{N(X^{+m+1})}{N(X^{+m})} = \frac{\zeta T_e}{(m+1)^2 I_m^2}\, 10^{3-5040 I_m/T_e} \tag{90}$$

where ζ is the number of electrons in the ion with ionization potential I_m; this gives $N(He^+)/N(He) = 1$, 4×10^{-4}, and 3×10^{-6} for $T_e = 10^4$, 10^5, and 10^6 K respectively. The optical depth allowing for cosmological streaming is given by an equation similar to (87) above,

$$\tau_L = -9 \times 10^{-10} \frac{N(He^+)}{N(He)} \frac{H_0^3 \Omega^2}{\nu^2 T_e^{3/2}} b_n \left(\frac{\Delta b}{b_n}\right) \tag{91}$$

For $H_0 = 100$ km sec^{-1} mpc^{-1}, $\Omega = 1$, $\nu = 10$ MHz, and $T_e = 10^6$ K, this gives $\tau_L \sim 3 \times 10^{-11}$, and for $T_e = 5 \times 10^4$ K, perhaps the best case, $\tau_L \sim 6 \times 10^{-10}$. It therefore seems clear that these lines will be undetectable, unless $\Omega \gg 1$, or unless the intergalactic medium is highly inhomogeneous.

8. Conclusions

Masing in recombination lines is most important at low frequencies, and especially for low-density plasmas. Indeed were it not for this masing, these recombination lines would scarcely be detectable at all.

An otherwise opaque plasma cloud may be transparent or even provide amplification at the frequency of a recombination line to radiation originating behind the cloud. These effects are greatest when the electron temperature is low and the emission measure high, conditions which may prevail in the cold cloud component of the interstellar medium. Amplification of background radiation could conceivably exceed 100 per cent in some cases. The optimum frequency would appear to lie in the range 50–200 MHz, where the non-LTE effects are greatest, the opacities substantial, and strong continuum sources abound.

The hot intercloud component of the interstellar medium should also give rise to detectable recombination lines. Hydrogen recombination lines may be as strong as one per cent of the background source intensity, and absorption lines due to other elements may be as strong as $10^{-4} T_0 - 10^{-3} T_0$ because of enormous overpopulation of the relevant energy levels due to dielectronic recombination. The best frequencies are again $\sim$ 50–200 MHz. The intergalactic medium is unlikely to emit detectable low-frequency recombination lines unless its density is considerably greater than the critical cosmological value; optimal frequencies are in the range 1–100 MHz for lines of both hydrogen (emission) and helium (absorption).

There have been few attempts to detect recombination lines at frequencies below 500 MHz, and most of these have been above 400 MHz with the emphasis on *ordinary* recombination lines from nearby HII regions. Observations of recombination lines below 200 MHz would permit the study of the phenomenon of negative absorption at those frequencies where it is most pronounced, and provide information regarding the relevant physical processes involved, particularly the electron-atom collisional cross-sections. They might facilitate separation of the hot and cold components of the interstellar medium because of the exponential dependence on temperature, and the investigation of the properties of the cold cloud component in particular. And finally it may be possible in some cases to study the spectra of galactic radio sources below the frequencies at which absorption in the continuum would otherwise completely obscure them.

Acknowledgements

I am greatly indebted to V Radhakrishnan for many suggestions and hours of stimulating discussions. The computations were done with the IBM 360/44 and 370/155 computers of the Indian Institute of Science (Bangalore) and the Indian Institute of Technology (Madras) respectively, and I am most grateful for the generous cooperation of the staff at these computer centres.

References

Aller L H 1953 *Astrophysics: The Atmospheres of the Sun and Stars* (Ronald Press, N.Y.)
Banks D, Percival I C and Richards D 1973 *Astrophys. Letters* **14** 161
Baranger M 1958 *Phys. Rev.* **112** 855
Berger P S and Simon M 1972 *Astrophys. J.* **171** 191
Bignell R C 1973 *Astrophys. J.* **186** 889
Brocklehurst M 1970 *Mon. Not. R. Astron. Soc.* **148** 417
Brocklehurst M 1971 *Mon. Not. R. Astron. Soc.* **153** 471
Brocklehurst M 1973 *Astrophys. Lett.* **14** 81
Brocklehurst M and Seaton M J 1972 *Mon. Not. R. Astron. Soc.* **157** 179
Burgess A 1958 *Non. Not. R. Astron. Soc.* **118** 477
Burgess A and Summers H P 1969 *Astrophys. J.* **157** 1007
Cesarsky D A and Cesarsky C J 1973 *Astrophys. J.* **184** 83
Chandrasekhar S 1960 *Radiative Transfer* (Dover Publ., New York)
Dulk G A and Slee O B 1972 *Aust. J. Phys.* **25** 429
Dupree A K 1969 *Astrophys. J* **158** 491
Dupree A K 1972*a* *Astrophys. J.* **173** 293
Dupree A K 1972*b* *Astrophys. Lett.* **12** 125
Field G B 1972 *Ann. Rev. Astron. and Astrophys.* **10** p. 227
Field G B, Goldsmith D W and Habing H J 1969 *Astrophys. J.* **155** 449
Flannery M R 1970 *Astrophys. J.* **161** L41
Gayet R 1970 *Astron. and Astrophys.* **9** 312
Goldberg L 1966 *Astrophys. J.* **144** 1225
Griem H R 1967 *Astrophys. J.* **148** 547
Harris D L 1948 *Astrophys. J.* **108** 112
Hjellming, R M, Gordon C P and Gordon K J 1969 *Astron. and Astrophys.* **2** 202
Landecker T L and Wielebinski R 1970 *Aust. J. Phys. Astrophys. Suppl.* No. 16
Lockman F J and Gordon M A 1973 *Astrophys. J.* **182** 25
Menzel D H 1937 *Astrophys. J.* **85** 330
Menzel D H 1968 *Nature* **218** 756
Menzel D H and Pekeris C L 1935 *Mon. Not. R. Astron. Soc.* **96** 77
Mezger P G and Hoglund B 1967 *Astrophys. J.* **147** 490
Milne D K 1970 *Aust. J. Phys.* **23** 425
Oster L 1961 *Rev. Mod. Phys.* **33** 525
Oster L 1970 *Astron. and Astrophys.* **9** 318
Peach G 1972 *Astrophys. Lett.* **10** 129
Posener D W 1959 *Aust. J. Phys.* **12** 184
Radhakrishnan V and Goss W M 1972 *Astrophys. J. Suppl.* No. **203** 161
Seaton M J 1959 *Mon. Not. R. Astron. Soc.* **119** 81
Seaton M J 1964*a* *Mon. Not. R. Astron. Soc.* **127** 177
Seaton M J 1964*b* *Planet Space Sci.* **12** 55
Shaver P A 1970 *Astrophys. Lett.* **5** 167
Shaver P A and Goss W M 1970 *Aust. J. Phys. Astrophys. Suppl.* No. 14, 133
Twiss R Q 1958 *Aust. J. Phys.* **11** 564